Published as: *Science*. 2008 June 6; 320(5881): 1336–1341.

Intersection of the RNAi and X-inactivation pathways

Yuya Ogawa, **Bryan K. Sun**, and **Jeannie T. Lee***
Dept. of Molecular Biology, Massachusetts General Hospital, Dept. of Genetics, Harvard Medical School, Howard Hughes Medical Institute, Boston, MA 02114

Abstract

In mammals, dosage compensation is achieved by X-chromosome inactivation (XCI) in the female. The noncoding *Xist* gene initiates silencing of the X, while its antisense partner *Tsix* blocks silencing. The complementarity of Xist and Tsix RNAs has long suggested a role for RNAi. Here, we report that murine Xist and Tsix form duplexes *in vivo*. During XCI, the duplexes are processed to small RNAs, most likely on the active X (Xa) in a Dicer-dependent manner. Deleting *Dicer* compromises small RNA production and de-represses *Xist*. Furthermore, without Dicer, Xist RNA cannot accumulate and H3-K27 trimethylation is blocked on the inactive X (Xi). Intriguingly, the defects are partially rescued by truncating Tsix. Thus, XCI and RNAi intersect, downregulating *Xist* on Xa and spreading silencing on Xi.

X-chromosome inactivation (XCI) (1) balances X-chromosome dosages between XX and XY individuals. XCI is initiated by *Xist* (2,3) and opposed by *Tsix* (4). How *Xist* induces XCI on Xi and how *Tsix* stably silences *Xist* on Xa remain two unanswered questions. A role for RNA-interference (RNAi) has long been speculated. RNAi refers to the repressive influence of double-stranded RNA (dsRNA) on gene transcription and transcript stability (5,6). Numerous similarities, including the involvement of noncoding RNAs, can be found between XCI and RNAi-silencing of constitutive heterochromatin. However, a Dicer (Dcr) efficiency has no obvious effect on maintaining Xi in T cells (7) and, although Xist and Tsix RNAs are perfectly complementary, dsRNAs had never been observed *in vivo*.

Here, we formally explore a role for RNAi in XCI. To search for small RNAs within *Xist/Tsix*, we performed Northern analysis in mouse embryonic stem (ES) cells, a model that recapitulates XCI during cell differentiation *ex vivo*, and in mouse embryonic fibroblasts (MEFs), post-XCI cells which faithfully maintain one Xi. At repeat A, a region of *Xist* required for silencing (8), we observed small RNAs at ~30 nt and ~37 nt in the Tsix orientation and at ~25 nt and ~35 nt in the Xist orientation (Fig. 1A). At *Xist* exon 7, small RNAs occurred between 24-42 nt on the Tsix strand and at ~25 and ~35 nt on the Xist strand (Fig. 1B). At the promoter, robust quantities of Tsix-strand small RNAs were observed (Fig. 1C). Small RNAs were also seen on the Xist strand, implying low level sense transcription must occur at the promoter. The integrity of all Northern blots were confirmed by miRNA292-as and tRNA controls (Fig. 1, S1). Intriguingly, the small RNAs were developmentally regulated, being unmeasurable in the pre-XCI (day 0, d0) and post-XCI (MEF) states and detectable only during XCI (d4, d10). Furthermore, small RNAs occurred in both XX and XY cells. For discussion purposes, we tentatively call them 'xiRNA' for their X-inactivation center origin, distinct from the smaller siRNAs and miRNAs.

To determine if xiRNA production depends on antisense expression, we investigated ES cells deleted for *Tsix* ($Tsix^{\Delta CpG}$) (4) and the *Tsix* regulator, *Xite* ($Xite^{\Delta L}$) (9). Deleting *Tsix* resulted

* Corresponding author: lee@molbio.mgh.harvard.edu.

in a dramatic reduction in antisense-strand xiRNA (Fig. 1D). A residual level of xiRNAs was still detectable, consistent with cryptic promoter activity in *Tsix*$^{\Delta CpG}$ (4). Deleting *Xite* likewise reduced antisense xiRNA levels, consistent with a requirement for *Xite* in transactivating *Tsix* (9). In the sense orientation, both deletions also compromised xiRNA production. Thus, small RNAs are indeed generated from *Xist/Tsix* and depend on *Tsix* and *Xite* expression.

The presence of xiRNAs implied that Tsix and Xist must exist as long duplex precursors. However, the developmental timing of xiRNA appearance is paradoxical: Although Tsix and Xist are biallelically expressed on d0, they become monoallelically expressed on opposite Xs during XCI (4). On d0, 3-5 copies/per chromosome of Xist RNA are present, while Tsix occurs at >10-fold molar excess (10-12). Upon XCI, Tsix is downregulated on Xi as Xist upregulates >30-fold. On Xa, Tsix persists as Xist is downregulated. How would dsRNA form when Tsix and Xist – both *cis*-limited – are on opposite chromosomes during XCI?

To determine if Tsix and Xist formed dsRNA, we devised an *in vivo* RNase protection assay based on differential susceptibility of ssRNA and dsRNAs to RNase A/T1. We permeabilized replicate preparations of d0 ES cells in a nondenaturing buffer containing DNAse I and RNAse, treated with RNase, and performed strand-specific RT-PCR on the protected RNAs. To confirm assay sensitivity, a positive control -- into which 1 copy/cell of *in vitro*-transcribed and annealed Tsix:Xist dsRNA is 'spiked' -- could readily be detected using this protocol (Fig. 2A,B). The abundant single-stranded Rrm2 and Gapdh transcripts were not amplified, indicating that our assay was specific for dsRNA. We consistently observed RNase-protected Xist and Tsix RNA strands in XX and XY ES cells, suggesting the presence of dsRNA (Fig. 2B). Real-time RT-PCR quantitation showed that ~16% of Xist and ~13% of Tsix were protected (Fig. 2C). As expected of duplexes, approximately equal stoichiometric ratios of the two strands were present in the RNase-protected fraction. Kinetic analysis revealed decreasing amounts of dsRNA during differentiation in XX and XY cells (Fig. 2D). Thus, steady state quantities of both dsRNA and xiRNA are developmentally regulated, but in an opposite manner.

The inverse correlation over time raised the possibility that dsRNA is processed to xiRNA. To address potential allelic differences, we performed allele-specific RNase protection assays using two genetically marked female ES cell lines – wildtype 16.7, which carries Xs from *Mus castaneus* (X^{cas}) and *M. musculus* (X^{mus}) and undergoes random XCI (with a natural 30:70 specific-specific bias (*13*)); and *Tsix*$^{\Delta CpG}$/+ mutants, which harbors a *Tsix* deletion on X^{mus} (4) and therefore always inactivates X^{mus} in the 16.7 background. Total Tsix RNA (no RNase treatment) decreased >10-fold over time, but a low residual level could still be detected at d4 and d10 as expected (data not shown) (4,9,14). From this residual pool, using SNP-based allele-specific primers at position 3, we unexpectedly found that duplexed Tsix (RNase-protected) in *Tsix*$^{\Delta CpG/+}$ cells predominantly originated from Xi (X^{mus}) (Fig. 2E) – the X on which the major *Tsix* promoter is deleted. Likewise, the Xist strand found in duplex form originated from Xi. Thus, Tsix:Xist duplexes are detected primarily from Xi.

Duplexes may form only on Xi, or they may form on both Xs but be stable only on Xi. The latter is especially intriguing, considering the inverse kinetic relationship between the appearance of long dsRNA versus xiRNA. Could dsRNA be processed to xiRNA on Xa? Several observations favored this idea. First, dsRNA was selectively lost from Xa. Second, xiRNA production depended on *Tsix*, a gene expressed from Xa on d4-d10. Finally, despite lacking Xi, XY cells produced xiRNAs.

Because dsRNAs are substrates for Dcr, we tested Dcr's role by deleting *Dcr*'s RNAseIII domain in female ES cells (15) (Fig. S2). Because Dcr-/- cells are known to grow poorly (15), we introduced a *Dcr* transgene expressed at ≪5% of wildtype levels (Fig. 3A,B) and improved growth of Dcr-deficient clones (henceforth dubbed Dcr-/-). Northern analysis

revealed diminished xiRNA levels (Fig. 3C,D), suggesting that xiRNA production depends on Dcr. All tested *Dcr*-deficient clones behaved similar. Significantly, *Xist* expression prematurely increased 5- to 10-fold in pre-XCI cells (Fig. 3B), implying increased *Xist* transcription or greater RNA stability. Male Dcr-/- clones likewise showed significant Xist de-repression on d4 (Fig. S3). Thus, Dcr regulates xiRNA levels and antagonizes *Xist* upregulation in ES cells.

RNA immunoFISH analysis showed that Dcr has additional XCI effects. Despite elevated Xist levels, Xist could not 'coat' the X nor induce heterochromatic changes (Fig. 3E). On d10, Xist RNA accumulation occurred in only 0.4% of cells (n = 278) and H3-K27 trimethylation (H3-3meK27) in 0.7% (n = 278). By contrast in *Dcr* 2lox/- controls, Xist accumulated in 56.8% and H3-K27 trimethylation in 83.1% (n = 148). Moreover, the X-linked *Mecp2* gene failed to be dosage compensated in *Dcr*-/- cells, whereas it appropriately decreased 1.5- to 2-fold in controls (Fig. 3A). Therefore, in addition to local effects on *Xist*, Dcr also affected Xi globally, as formation of Xist and H3-3meK27 domains were compromised without Dcr.

Because XCI and cell differentiation are linked (16,17), the XCI defects might be explained by Dcr's pleiotropic effects on differentiation (15,18) rather than specific effects on XCI. Indeed, *Dcr*-/- clones differentiated poorly and continued to express Oct4 and Nanog pluripotency factors on d10 (Fig. 3A,F, Fig. S3). To determine if Dcr specifically affects XCI, we truncated Tsix by inserting a polyA cassette in *Dcr*-/- cells (Fig. S4), reasoning that disabling *Tsix* – which negatively regulates *Xist* — might overcome the failure to accumulate Xist RNA. As expected, *Dcr*-/- *Tsix*-/+ double mutants (Dcr-TST) and *Tsix*-/+ controls (TST) showed truncated Tsix expression from X^{mus} and highly skewed XCI patterns (Fig. 4A). Although Dcr-TST cells continued to differentiate poorly (Fig. S5), total Xist levels were restored to nearly WT levels during differentiation (Fig. 4B). Furthermore, disabling Tsix partially restored Xist localization to Xi (Fig. 4C). Therefore, Dcr's effect on XCI can be genetically separated from its effect on cell differentiation.

Additionally, to the extent that Xist levels and localization were restored in Dcr-TST cells, H3-K27 trimethylation was only partly rescued in $Xist^+$ cells (Fig. 4D). In WT and TST controls, Xist accumulation was almost always accompanied by robust H3-K27 trimethylation. In contrast, 30-40% of $Xist^+$ Dcr-TST cells displayed weak or no H3-3meK27 foci, implying that H3-K27 trimethylation also depends on Dcr. These data showed that Xist accumulation and H3-K27 methylation are genetically separable. We conclude that Dcr intersects XCI in several ways. Locally, Dcr controls xiRNA and Xist expression. Globally, it regulates Xist accumulation and H3-K27 trimethylation on Xi.

In aggregate, our data suggest specific effects of RNAi on XCI (Fig. 4E). *Dcr* and *Tsix/Xist* genetically interact, as a second-site mutation in *Tsix* partially suppresses the *Dcr*-/- effect on *Xist*. We propose that Tsix:Xist duplexes initially form on both Xs. During XCI, continued expression of Tsix on Xa would lead to dsRNA processing to xiRNAs, which would locally repress *Xist in cis* – an idea reminiscent of transcriptional gene silencing (TGS) (6,19-21). Consistent with 'allele-specific TGS' at *Xist*, RNA-directed DNA methylation by *Tsix* has been proposed (10). Indeed, here we found that abrogating Dcr and/or Tsix resulted in decreased methylation at the 5′ end of *Xist* (Fig. 4F). By our model, extremely low Tsix and Xist expression might be sufficient to maintain TGS on Xa in post-XCI cells (19). On Xi, chromosome-wide accumulation of Xist RNA and H3-K27me3 depends on Dcr. These ideas support the emerging concept of nuclear RNAi processes in mammals (20,21). Because Dcr is not known to cleave RNAs to 25-42 nt, the observed effects on XCI may be partially indirect. Alternatively, Dcr may have novel properties yet to be discovered in mammals. XCI now provides a new system in which to investigate RNAi processes.

Supplementary Material

Refer to Web version on PubMed Central for supplementary material.

References and Notes

1. Lyon MF. Nature 1961;190:372. [PubMed: 13764598]
2. Brown CJ, et al. Cell 1992;71:527. [PubMed: 1423611]
3. Penny GD, Kay GF, Sheardown SA, Rastan S, Brockdorff N. Nature 1996;379:131. [PubMed: 8538762]
4. Lee JT, Lu N. Cell 1999;99:47. [PubMed: 10520993]
5. Fire A, et al. Nature 1998;391:806. [PubMed: 9486653]
6. Grewal SI, Elgin SC. Nature 2007;447:399. [PubMed: 17522672]
7. Cobb BS, et al. J Exp Med 2005;201:1367. [PubMed: 15867090]
8. Wutz A, Rasmussen TP, Jaenisch R. Nat Genet 2002;30:167. [PubMed: 11780141]
9. Ogawa Y, Lee JT. Mol Cell 2003;11:731. [PubMed: 12667455]
10. Sun BK, Deaton AM, Lee JT. Mol Cell 2006;21:617. [PubMed: 16507360]
11. Buzin CH, Mann JR, Singer-Sam J. Development 1994;120:3529. [PubMed: 7529677]
12. Shibata S, Lee JT. Hum Mol Genet 2003;12:125. [PubMed: 12499393]
13. Avner P, et al. Genet Res 1998;72:217. [PubMed: 10036978]
14. Shibata S, Lee JT. Curr Biol 2004;14:1747. [PubMed: 15458646]
15. Murchison EP, Partridge JF, Tam OH, Cheloufi S, Hannon GJ. Proc Natl Acad Sci U S A 2005;102:12135. [PubMed: 16099834]
16. Monk M, Harper MI. Nature 1979;281:311. [PubMed: 551278]
17. Lee JT. Science 2005;309:768. [PubMed: 16051795]
18. Kanellopoulou C, et al. Genes Dev Feb 15;2005 19:489. [PubMed: 15713842]
19. Volpe TA, et al. Science 2002;297:1833. [PubMed: 12193640]
20. Kim DH, Villeneuve LM, Morris KV, Rossi JJ. Nat Struct Mol Biol 2006;13:793. [PubMed: 16936726]
21. Morris KV, Chan SW, Jacobsen SE, Looney DJ. Science 2004;305:1289. [PubMed: 15297624]
22. We thank G. Hannon for the *Dcr* targeting construct and Dcr2lox/- male ES cells; N. Lau for technical advice; and M. Anguera, J. Erwin, S. Namekawa, B. Payer, and J. Zhao for careful critique of the manuscript. Y.O. is especially indebted to A. Ogawa for her support. This work is funded by the Medical Scientist Training Program (B.K.S.) and the NIH and HHMI (J.T.L.).

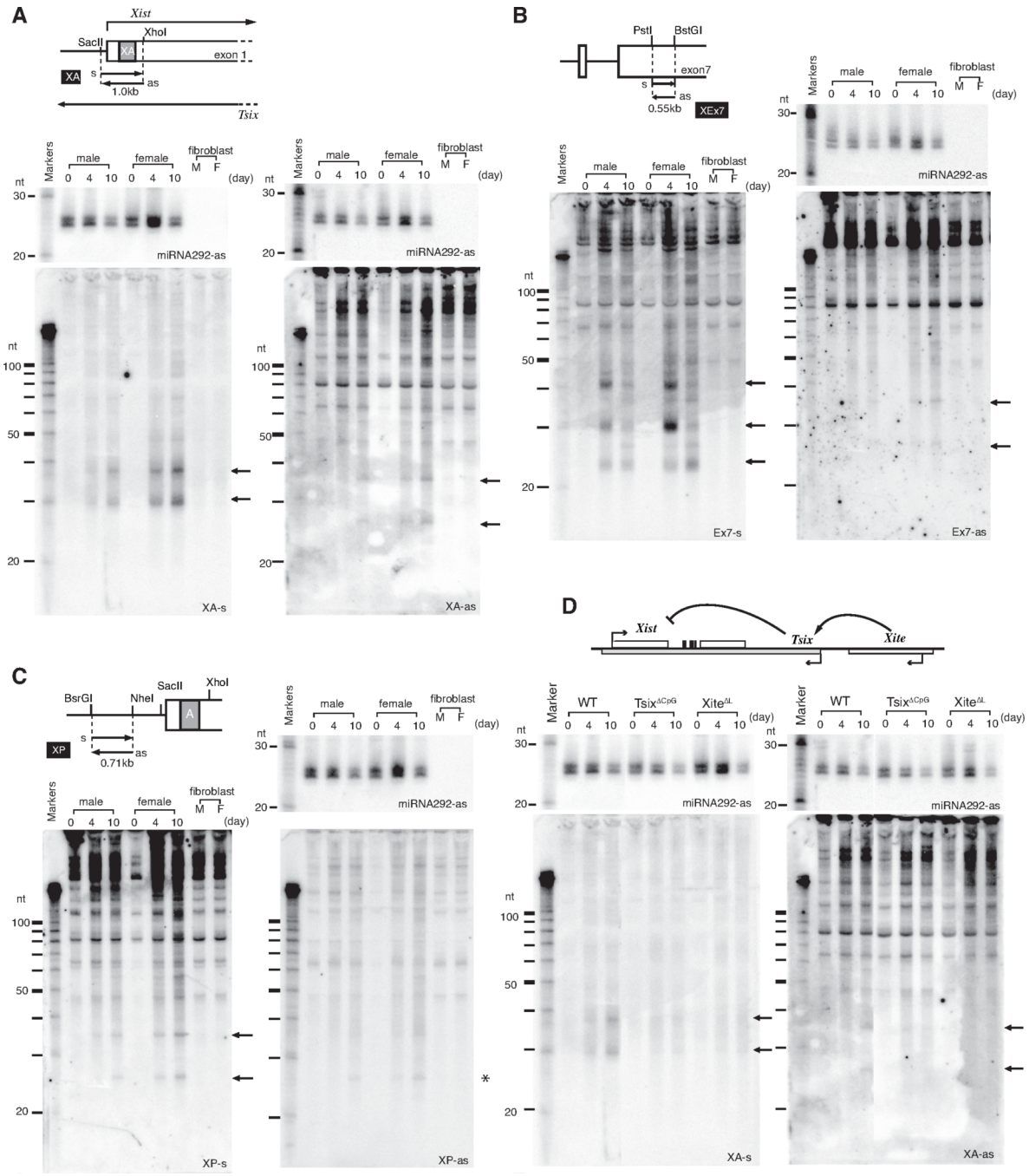

Figure 1. Small RNAs derived from *Tsix/Xist*

(A) xiRNAs from *Xist* repeat A (XA) region (map) detected by Northern analysis. Sense (s) and antisense (as) riboprobes detect Tsix and Xist, respectively. miR292-as controls are shown on same blots. M, male. F, female.

(B) Northern analysis of xiRNAs from *Xist* exon 7.

(C) Northern analysis of *Xist* promoter region.

(D) Northern analysis of mutant cells. WT lanes identical to those in panel A (concurrent analysis).

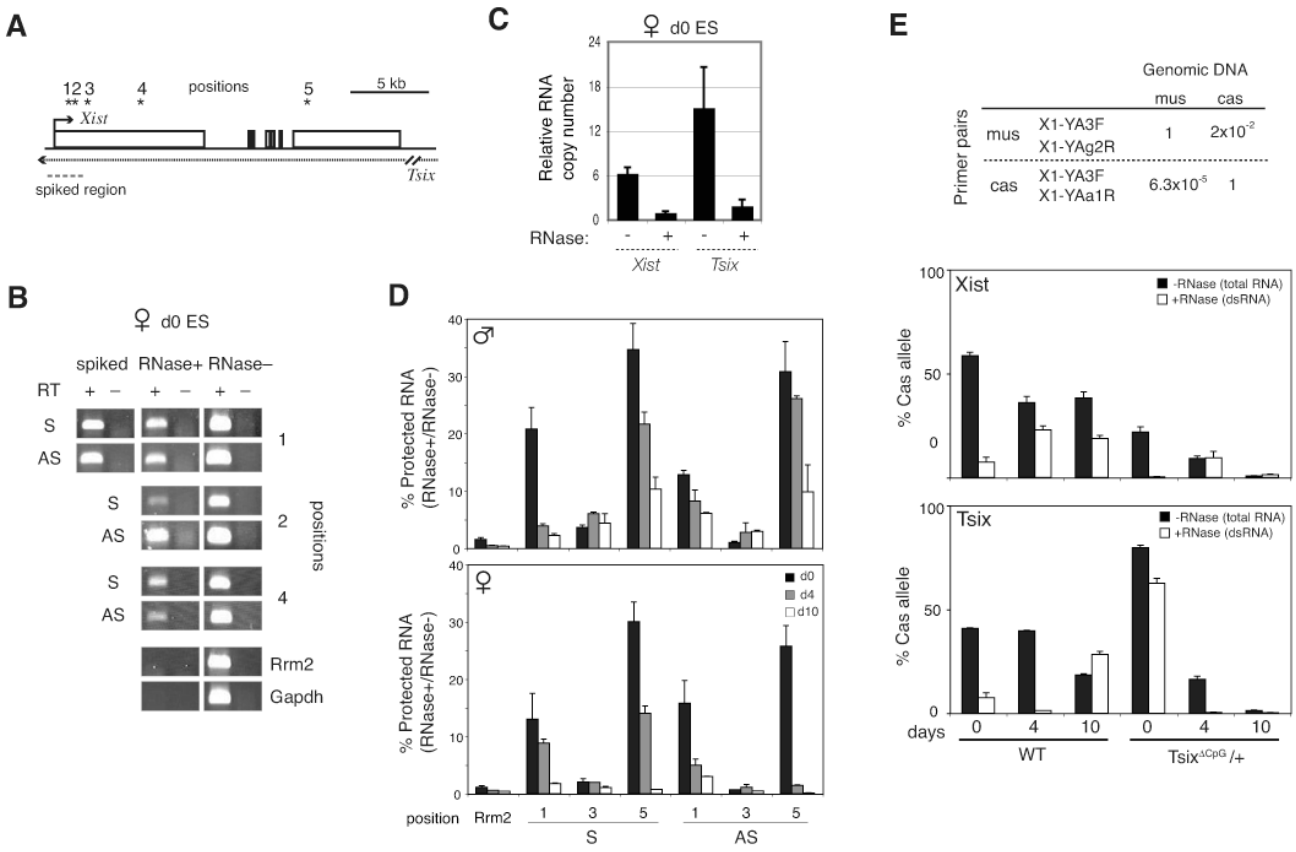

Figure 2. Tsix and Xist RNA form long duplexes *in vivo*

(A) Map of *Tsix/Xist* and primer pairs (*).

(B) *In vivo* RNAse protection assay. S, sense. AS, antisense.

(C) Relative quantities of Xist and Tsix in duplexes measured at position 2 (bp 1206-1337 of *Xist*) by strand-specific real-time RT-PCR of protected RNA (RNAse+) as compared to total levels (RNAse–). Quantities are standardized to Xist in the Xist-Tsix duplex (Xist, RNAse+ = 1). Error bars=one standard deviation (SD) in triplicate reactions.

(D) Quantities of protected Tsix or Xist RNAs (RNase+) relative to total Tsix or Xist (RNase-) for *in vivo* RNAse protection assays. Error bar=1SD, triplicate reactions.

(E) *In vivo* RNAse protection assays to test allelic origin of dsRNA using strand-specific, allele-specific realtime RT-PCR with SNP-based primers for X^{cas} or X^{mus} alleles (Table). PCR of control genomic DNA shows high specificity (98% for mus, >99.99% for cas). Error bar=1SD, triplicate reactions. For test samples, the mus and cas fractions were amplified separately, normalized to genomic DNA (X^{cas}: X^{mus} =1:1), and plotted as a function of time. %cas = [X^{cas} RNA/ (X^{cas} RNA + X^{mus} RNA)] × 100. Because the bars show relative allelic fractions, quantities are only comparable within a single timepoint.

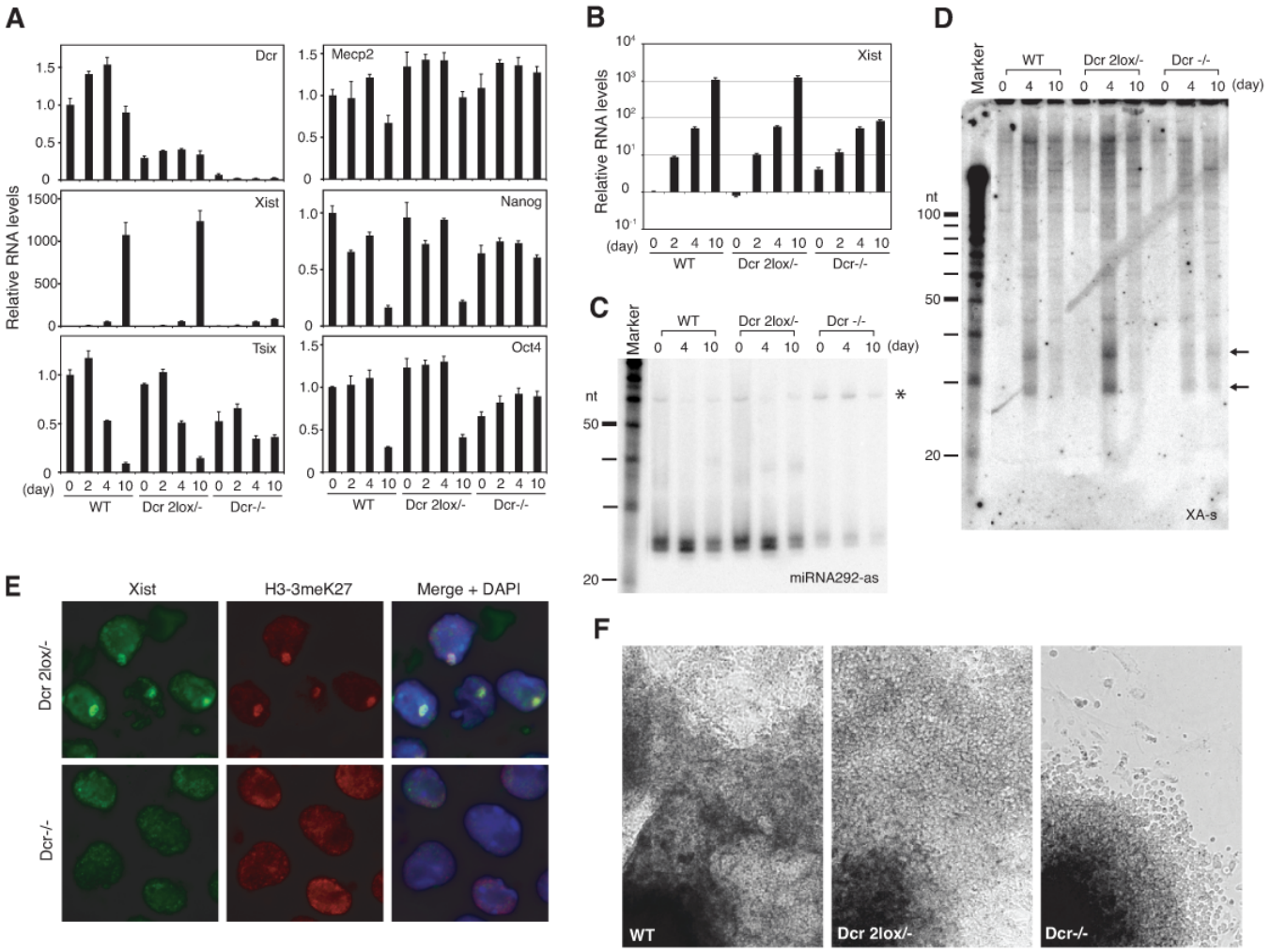

Figure 3. *Dcr* deficiency impairs xiRNA production and XCI

(A) Quantitative realtime RT-PCR of indicated transcripts normalized to β-actin.

(B) Xist quantitation plotted on a log scale.

(C,D) Northern analyses of miRNA292-as control (C) and xiRNAs (D) in mutant cells. Note accumulation of miRNA292-as precursors (*) in *Dcr*-/- cells.

(E) Immuno-RNA FISH for Xist and H3-3meK27 on d10. DAPI, blue.

(F) Phase contrast images of d10 EB.

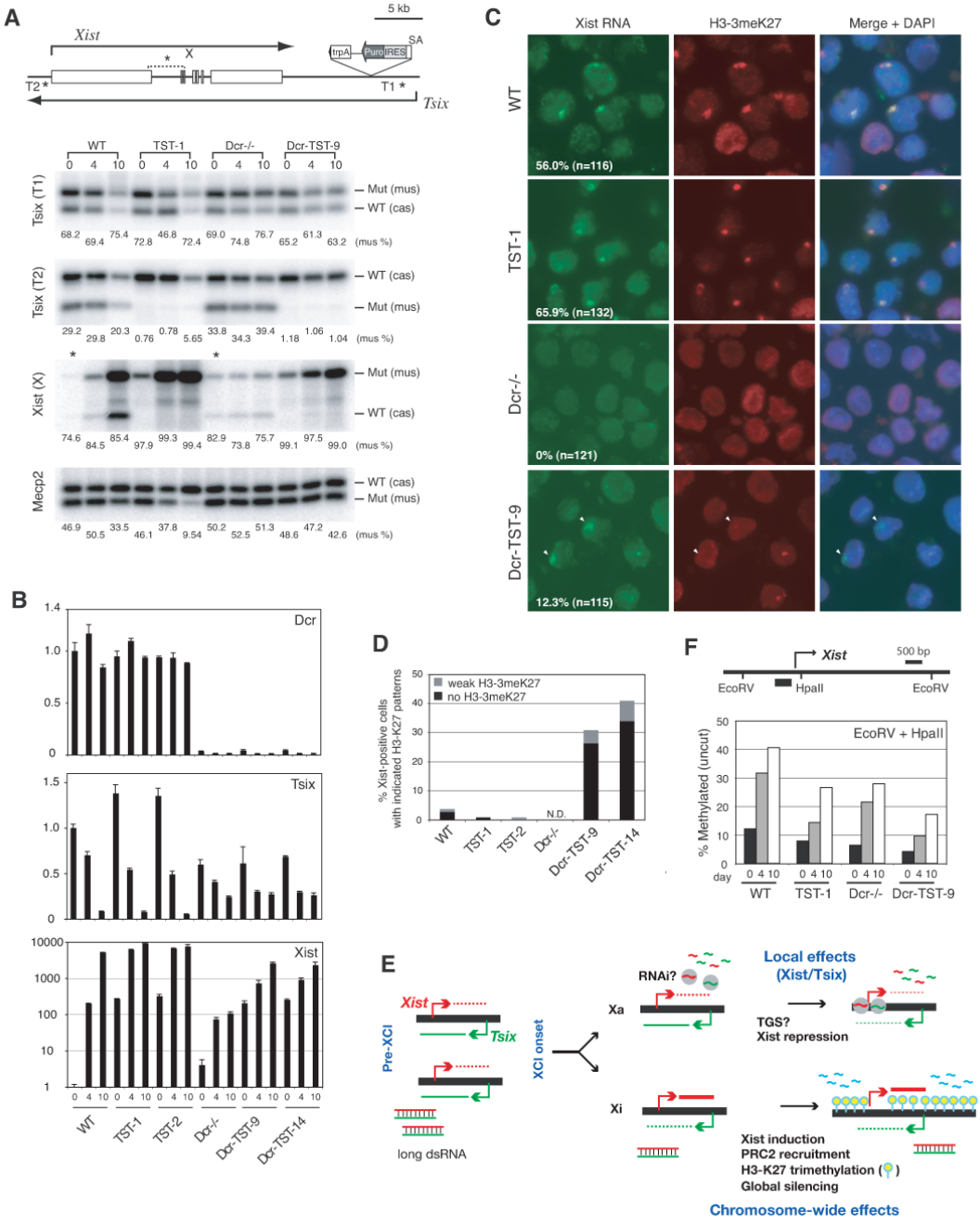

Figure 4. *Tsix* genetically interacts with *Dcr*

(A) Allele-specific RT-PCR analysis. All RT- reactions were negative (not shown). Xist d0 samples (asterisks) were 10-fold overloaded to visualize low expression.

(B) Realtime RT-PCR of indicated transcripts, each normalized to β-actin.

(C) Immuno-RNA FISH for Xist and H3-3meK27 domains (arrowheads) on d10.

(D) Frequency of aberrant H3-3meK27 enrichment in the Xist^{+} subpopulation of indicated cell lines. n=100-150.

(E) Model: intersection of RNAi and XCI.

(F) Methylation-sensitive restriction analysis of the *Xist* promoter. Genomic DNA was digested with EcoRV or EcoRV+HpaII. % uncut (methylated) DNA at HpaII is plotted.